Journal of
Materials Chemistry A

Accepted Manuscript

This article can be cited before page numbers have been issued, to do this please use: Y. Wu, Y. Zhao, J. Liu and F. Wang, *J. Mater. Chem. A*, 2018, DOI: 10.1039/C8TA00029H.

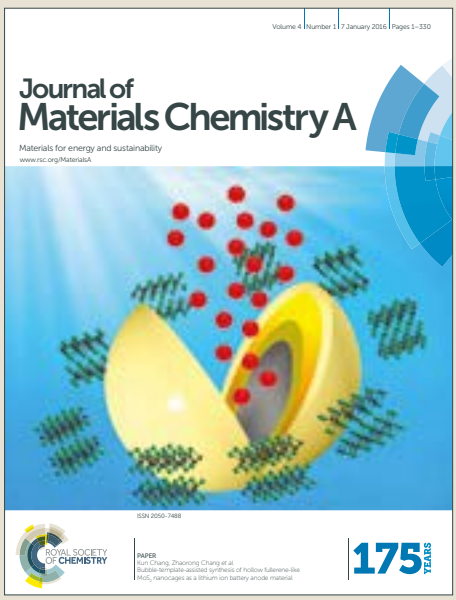

ROYAL SOCIETY OF CHEMISTRY

rsc.li/materials-a

View Article Online
DOI: 10.1039/C8TA00029H

Journal Name

ARTICLE

Adding refractory 5d transition metal W into PtCo system: An advanced ternary alloy for efficient oxygen reduction reaction

Received 00th January 20xx,
Accepted 00th January 20xx

DOI: 10.1039/x0xx00000x

www.rsc.org/

Yijun Wu, Yige Zhao, Jingjun Liu*, Feng Wang*

Tungsten (W), as one of the refractory 5d transition high-valency metals with unique physical and chemical properties, may substantially improve Pt-based alloys, providing superior electro-catalytic performance for the oxygen reduction reaction (ORR) that has been considered as the key cathode process in fuel cell automotives or portable devices. In this paper, we developed the graphene-supported Pt-Co-W ternary alloy, by using a facile one-pot polyol co-reduction of the above three metal. In the 0.1M $HClO_4$ solution, the obtained Pt-Co-W ternary alloy exhibits a surprisingly high specific activity of 3.41 $mA{\cdot}cm^{-2}$, which is 4.3 times higher than that of the well-known Pt-Co binary alloy (0.80 $mA{\cdot}cm^{-2}$) and 13 times over that obtained by the state-of-the-art Pt/C (0.27 $mA{\cdot}cm^{-2}$). The mass activity of the alloy is 2.25 $A{\cdot}mg^{-1}_{Pt}$, which is 4.2 times higher than that of the Pt-Co binary alloy (0.53 $A{\cdot}mg^{-1}_{Pt}$) and 12 times higher than that obtained by the state-of-the-art Pt/C (0.19 $A{\cdot}mg^{-1}_{Pt}$), at 0.9 V versus a reversible hydrogen electrode (RHE). The remarkably enhanced ORR activity can be attributed to the incorporating of small amount W into the Pt-Co alloy system at atomic level. The added W atoms can not only strengthen the chemical adsorption of oxygen molecules but also significantly facilitate the desorption of the oxygenated species on the active Pt sites in this ternary alloy, because W has stronger electronegativity, higher unsaturated 5d orbitals, and higher valency coordinated with these oxygenated groups. Therefore, introducing the cheap refractory transition metals like W into Pt-based binary alloys may open a door to fabricate the efficient next-generation ternary catalysts for the ORR.

1. Introduction

Proton exchange membrane fuel cell (PEMFC), as one of the most promising clean energies alternative to traditional fossil fuels, can be widely used in the fields of new energy vehicles, electric propulsion ships, portable devices and so on.[1] One of the major obstacles for the commercial application of PEMFC is the sluggish kinetics of the oxygen reduction reaction (ORR).[2,3] The metal Pt is currently considered as the best choice to overcome the barrier due to its high activity, but the high cost and poor durability restrict its practical application.[4-6] In recent years, many research results suggest that Pt alloying with a transition metal (such as Co, Fe, Ni, Cu[7-11]) can not only reduce the usage amount of the expensive Pt, but also substantially improve the catalytic activity by two to three times, relative to that of pure Pt. Among these alloys mentioned above, the bimetallic platinum-cobalt (Pt-Co) systems have been paid great attentions due to their best catalytic activity and durability during the ORR.[12-16] Nevertheless, the activity and stability for state-of-the-art Pt-Co alloys are still not good enough, which have not meet the harsh requirements of large-scale practical application in new energy vehicles. For the new energy automotive, a catalyst with an at least four-fold specific activity over the Pt deems crucial.[17]

Fabricating Pt-based ternary alloys may open a door to further improve the ORR activity, compared with binary alloy systems, according to the recent results.[18-24] For example, Srivastava et al.[15] suggested that the mass activity of Pt-Co-Cu catalyst was four-fold over the Pt/C catalyst. Ozenler et al. [25] showed that the mass activity of Pt-Co-Sn catalyst was approximately 5 times higher than that of the Pt/C catalyst. Tan et al.[18] found that the specific activity of Pt-Co-Fe catalyst exhibited 350% higher than that of the Pt/C catalyst. The improved ORR performance may be attributed to the electronic or ligand effects, raised by the added third transition metals into the Pt-based alloys.[26,27] Recently, Huang et al.[21] fabricated molybdenum (Mo)-surface-doped octahedral Pt_3Ni nanostructure on a carbon black and suggested that the trimetallic catalyst displays a surprising ORR activity that is much higher than that of a commercial Pt/C catalyst. However, the synthesized Pt_3Ni alloys doped with other transition metals, such as Fe, Co, Mn, V, and Cr, exhibit relatively poor ORR activity with respect to the above Mo-doped Pt-Ni alloy. Therefore, it is clear that introducing an appropriate and suitable third transition metal into Pt-based binary alloys is very important to achieve the remarkable enhancement of the ORR activity. However, it is hard to select an ideal metal from

[a] State Key Laboratory of Chemical Resource Engineering, Beijing Key Laboratory of Electrochemical Process and Technology for Materials, Beijing University of Chemical Technology, Beijing 100029 (China)

Electronic Supplementary Information (ESI) available: See DOI: 10.1039/x0xx00000x

View Article Online
DOI: 10.1039/C8TA00029H

various transition metals to fabricate the novel ternary alloys because of the lack experimentally or theoretically relevant data in this aspect. One of the major difficulties lies in that the detail ORR mechanism over the ternary alloys remains unclear by now.

Tungsten (W), as one of the refractory 5d transition metals like Ta, Hf, and Re, has a very high melting point (about 3422 ºC), and exhibits many unique physical and chemical properties, such as strong electronegativity, highly unsaturated 5d orbitals, and high-valency states coordinated with oxygen-containing groups (e.g.: O, OH, OOH).[28-32] Based on these unique characteristics of the metal, adding it into Pt-Co alloy system may offer an efficient strategy to remarkably improve the electrocatalytic performance. Firstly, as it is added into the Pt-Co binary alloy, the covalent electron density of Pt component will decrease owing to the higher electronegativity of W (2.36) than that of Pt (2.28) and Co (1.88).[33] It brings about the increase in 5d vacancies of the Pt, which contributes the donation of 2π electrons from O_2 to Pt.[25] As a result, the O_2 chemical adsorption becomes stronger and the O-O bonds are easier to split, which is positive to the improved intrinsical activity of Pt in the catalysts. Secondly, W has the highly unsaturated 5d orbitals ($5d^4 6S^2$), which can be expected to result in the charge redistribution from Pt to W atoms through a strong electronic hybridization between the two metals. So that the d-band center of Pt will upshift relative to the Fermi level, which also favor the ORR.[34] Thirdly, high-valency W is supposed to have a rapid change between the high and low ion valences, which renders the W atoms to be active for chemisorbed oxygen-containing groups (e.g.: O, OH, OOH).[33,35,36] So, the W atoms are significantly easy to combine with these oxidic species generated by the ORR, resulting in one or more oxygen-containing group ligands bonded with the metal atoms. More importantly, the adsorption of these ligands on the W atoms is stronger than that of Pt or Co, which can result in the easy divorce of the oxidic intermediates adsorbed on the Pt surface, caused by a lateral repulsion between these oxygenated species.[18] As a result, more electrochemically active sites available for the ORR. At last, the third transition metal also stabilizes the Pt-based systems and prevents the dissolution of Pt atoms,[37-40] which is favorable for enhancement of the durability for the catalysts. Therefore, it is clear that incorporating cheap refractory transition metals like W into Pt-Co bimetallic systems may be a smart way to substantially improve the ORR activity. However, it has been paid a little attention by now, which hinders the development of high cost-efficient ORR catalysts.

Herein, graphene-supported Pt-Co-W ternary alloy nanoparticles (Pt-Co-W/C) were prepared by co-reduction of the above three metal, using a facile one-pot polyol reduction method at 130 ℃. In an acidic environment, electrochemical tests showed that the ternary Pt-Co-W alloy exhibits superior ORR activity to Pt-Co catalyst or a state-of-the-art commercial Pt/C. The origin of the improved electro-catalytic performance can be attributed to the introducing of low metal W into the Pt-Co binary alloy. This work proposed a novel and simple strategy to further improve the activity and stability of Pt-based catalysts. A possible ORR mechanism on the synthesized Pt-Co-W ternary alloy was discussed in detail.

2. Experimental

2.1. Preparation of Pt-Co-W ternary alloy

In a typical polyol process, 50 mg of graphene (Chengdu zhongke era, with 1-3 nm thickness) was added into 50 mL of ethylene glycol (EG), followed by the addition of 9.30 mL of H_2PtCl_6 (0.01 M) and 0.31 mL of $CoCl_2$ (0.1 M) solutions. Afterwards, 2.07 mL of $W(CO)_6$ (1.5 mM) was added into the suspension with all metal loading of 20 wt% in the carbon-supported Pt-Co-W ternary alloy, similar to the Pt-Co/C and the commercial Pt/C (the state-of-the-art 20 wt.% Pt,). Then, the pH value of mixture was adjusted to 10 with NaOH solution. After the vial was capped, the mixture was ultrasonicated for 30 minutes. Next, obtain homogeneous mixture was heated at 130 ℃ for 3 h in the oil bath. Lastly, the resulting solution was filtered and washed to get catalyst powder and the powder was dried at room temperature. The preparation of Pt-Co binary alloy catalyst is similar to the above preparation procedures without the addition of $W(CO)_6$.

2.2. Physical Characterizations

The morphologies of all alloy samples were studied by transmission electron microscopy (TEM, 2010 microscope, JEOL). The samples were prepared by dropping ethanol dispersion of catalysts on the TEM micro grids and dried under room temperature. The structure analysis of the samples was investigated by X-ray diffraction (XRD) with Cu KR radiation at λ=1.54 Å on a Philips Xpert X-ray diffractometer. The atom arrangement was researched by high-angle annular dark-field scanning transmission electron microscopy (HAADF-STEM, JEOL ARM 200F) at 200 KV and by energy dispersive X-ray spectroscopic (EDX). X-ray photoelectron spectra (XPS, ESCALAB 250) were obtained from a monochromator (Al KR source) calibrated with respect to the C (1s) peak at 284.6 eV. The real atomic ratio of Pt, Co and W atoms in the synthesized Pt-Co-W ternary alloy is approximately 72: 26: 2 while the corresponding fraction of Pt and Co atoms in the Pt-Co binary alloy is approximately 72: 28, as determined by inductively coupled plasma atomic emission spectroscopy (ICP-AES). Moreover, For the above trimetallic and bimetallic materials, the weight fraction of all the metals to carbon is about 20 wt.%, checked by inductively-coupled mass spectrometry. For this analysis, 5 mg of the above alloy sample was dissolved into 15 ml HCl/HNO_3 (3:1) solution. Based on the concentration of each of metal ions, determined by ICP-AES measurments, the weight fraction of the metals to carbon can be calculated.

2.3. Electrochemical Characterizations

View Article Online
DOI: 10.1039/C8TA00029H

The conventional three-electrode system was used to explore the electro-catalytic characteristics of all samples at room temperature. The cyclic voltammetry (CV) was used to obtain the electrochemically active surface areas (ECSAs) in an N_2-purged $HClO_4$ (0.1 M) solutions at a sweep rate of 50 $mV \cdot s^{-1}$. The catalytic activity and durability of catalysts were characterized by rotating ring electrode (RDE) in O_2-purged $HClO_4$ (0.1 M) solution with 1600 rpm at the scan rates of 5 $mV \cdot s^{-1}$. In this conventional system, the rotating disk electrode was used as working electrode. Pt foil was used as the counter electrode, and a saturated calomel electrode (SCE) was used as the reference electrode. For working electrode, 5 mg of Pt-Co-W catalyst (the total metal loading is 20wt%) was dispersed in 2 ml of alcohol and 100 μL of Nafion solution (5 wt%) ultrasonically, then 10 μL of the above suspension was loaded onto the glassy carbon electrode (S_{disk}=0.247 cm^2). The Pt loading of for all the Pt-Co-W and Pt-Co is 14.18 $\mu g_{Pt}/cm^2$ on the working electrode (glass carbon with geometric electrode area of 0.247 cm^2). Before RDE experiments, the reference electrode was calibrated by using the standard saturated calomel electrode. For studying the ORR pathway over the catalysts, we performed rotating ring-disk electrode (RRDE) measurements in the 0.1M $HClO_4$ solution saturated with O_2. The disk and the ring currents were in the negative scan direction and the ring potential was fixed at 0.5 V (vs. SCE). The recorded potential values are normalized by RHE, according to $E_{vs\ RHE} = E_{vs\ SCE} + 0.241\ V + 0.059 \times pH$.[41]

3. Results and discussion

3.1. Formation of ternary Pt-Co-W alloys

The graphene-supported ternary Pt-Co-W alloy nanoparticles (Pt-Co-W/C) were prepared by co-deposition of the H_2PtCl_6, $CoCl_2$ and $W(CO)_6$ as precursor salts, using ethylene glycol reduction method at different pH values. The schematic illustration of the facile one-pot fabrication of the graphene-supported Pt-Co-W ternary alloy is shown in Fig. 1A. The formation of the ternary alloy involves with the co-reduction of three metal elements (Pt, Co, W) by ethylene glycol as the reducing agent, which in return is oxidized into glycolic acid or glycolate anion as stabilizer in the solution at 130 ℃, depending on the solution pH.[34,38] As the pH increases, the stability of the glycolate anion increases accordingly, otherwise, the reducing ability of glycolic acid decreases until the reducing is lost.[35] So, the nanoparticle sizes of the alloys supported on graphene depend strongly on the solution pH, as evidenced by the results shown in Fig. S1. As the pH was fixed at approximately 10, the obtained Pt-Co-W alloy nanoparticles are highly dispersed on graphene without obvious agglomerates shown in Fig. 1B and C. The average size of the as-synthesized Pt-Co-W nanoparticles is about 2.9 nm shown in Fig.1D, which is almost similar to that of the Pt-Co binary alloy (2.6 nm) shown in Fig. S2. Besides, as illustated in the high-resolution transmission electron microscopy (HRTEM) image (Fig. 1E), the obtained Pt-Co-W alloy shows the well-

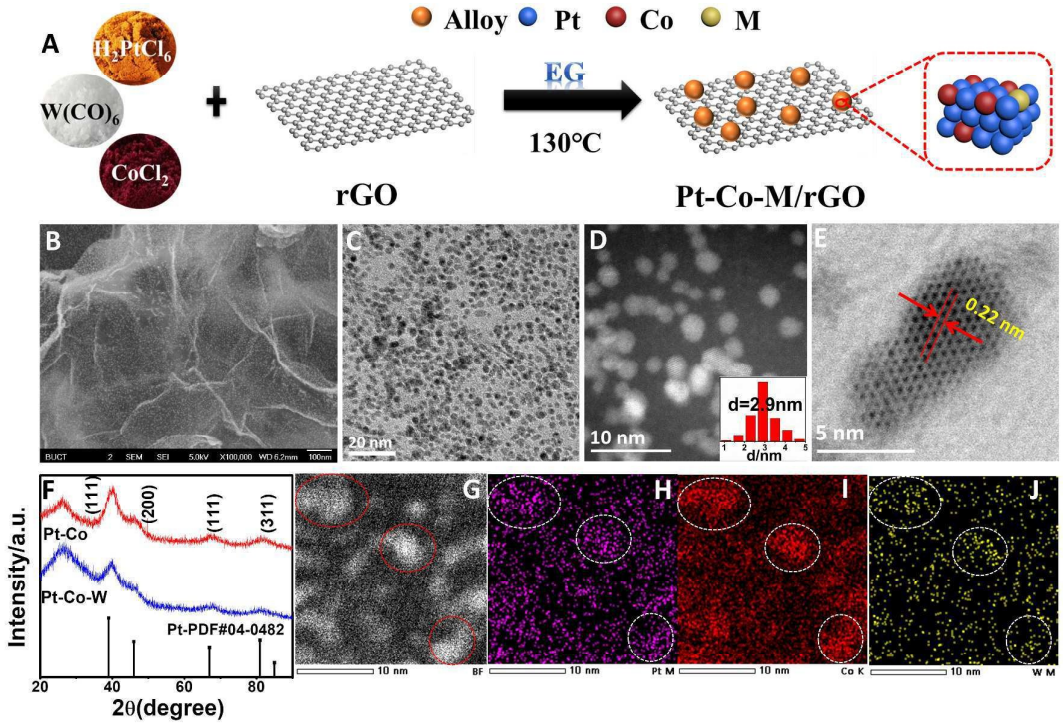

Fig. 1 (A) Schematic illustration of the one-pot fabrication of graphene-supported Pt-Co-W ternary alloy; **(B)** and **(C)** SEM and TEM images for the Pt-Co-W ternary alloy; **(D)** Annular dark-field STEM(ADF-STEM) image, insert: the size distribution of the alloy nanoparticles; **(E)** HRTEM image of individual particle; **(F)** XRD patterns of the alloy; **(G)** ADF-STEM image of the Pt-Co-W alloy; **(H-J)** Energy-dispersive X-ray (EDX) mapping of Pt, Co, W, respectively.

View Article Online
DOI: 10.1039/C8TA00029H

defined fringes with a lattice spacing of 0.22 nm, which is closely in agreement with that assigned for the Pt-Co binary alloy with a face-centered cubic (fcc) structure, indicating the formation of face-centered cubic Pt-Co-W ternary alloy.

In order to further prove the formation of the well-defined ternary Pt-Co-W alloy, X-ray diffraction pattern was performed for the sample and the obtained result is shown in Fig. 1F. As observed, except for the carbon peak at around 25°, the other four characteristic peaks correspond to the (111), (200), (220) and (311) planes characteristic of face-centered cubic (fcc) crystalline Pt-Co alloy. No peaks of pure Co and W or other miscellaneous peaks were observed here. Compared with pure Pt (JCPDS number: 04-0802), these characteristic peaks assigned to the alloy are obviously shifted to the higher angles, which further confirms the formation of the Pt-Co-W solid solution alloy. However, there is no clear shift of these diffraction peaks for the Pt-Co-W alloy, relative to the Pt-Co binary alloy shown in Fig. 1F. It can be attributed to the small content of the added W relative to the other two alloyed metals in this ternary alloy, as shown in Table S1. The real atomic ratio of Pt, Co and W in the Pt-Co-W is approximately 72: 26: 2, while the Pt/Co atomic ratio in the Pt-Co alloy is about 72: 28. To verify the doping of W into Pt-Co system,

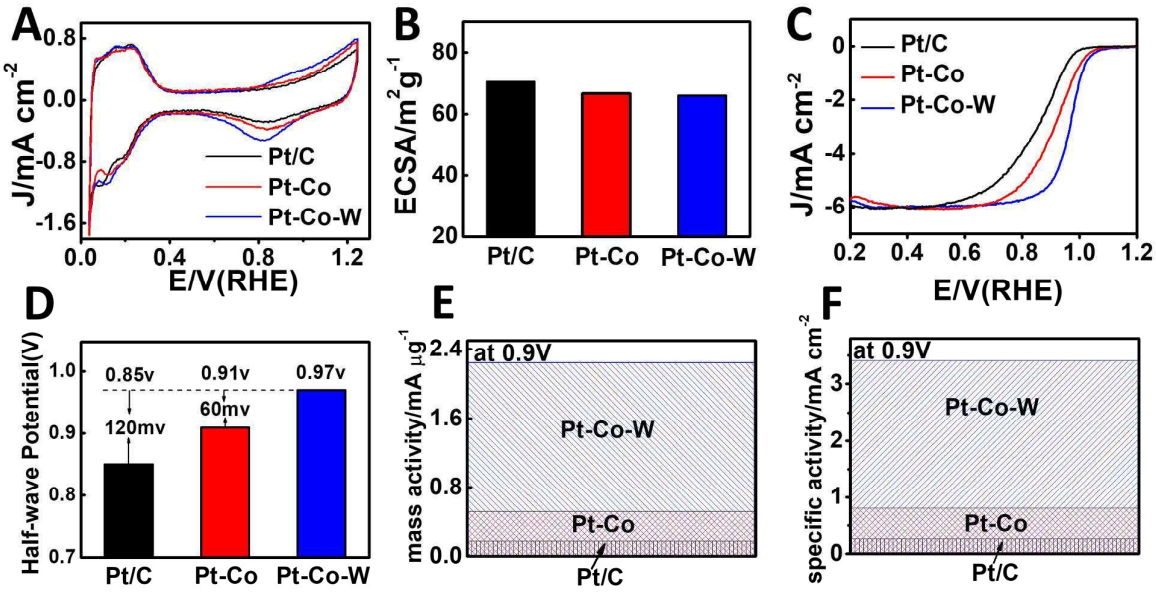

Fig. 2 (A) CV curves of various catalysts in an N_2-purged 0.1M $HClO_4$ solution with a sweep rate of 50 mV·s^{-1}; **(B)** The measured specific ECSA of various catalyst samples, (The current (J) was normalized by the area of the glassy carbon area (0.247 cm^2)); **(C)** RDE measurements on various catalysts in an O_2-purged 0.1M $HClO_4$ solution with a sweep rate of 5 mV·s^{-1} at 1600 rpm; **(D)** The recorded half-wave potentials of these catalysts; **(E)** The mass activities normalized by Pt loading at 0.9 V; **(F)** The specific activities (normalization by ECSAs) at 0.9 V.

Table 1. Catalytic activity of Pt-Co-W catalyst and other published catalysts (SA- Specific activity; MA- Mass activity; NA- not available).

	Catalyst	Based on H_{upd}					Based on CO stripping		
		ECSA (m^2/g_{Pt})	SA (mA/cm^2)		MA (A/mg_{Pt})		ECSA (m^2/g_{Pt})	SA (mA/cm^2)	
			@0.9 V	@0.95 V	@0.9 V	@0.95 V		@0.9 V	@0.95 V
This work	Pt-Co-W	65.9	3.41	0.97	2.25	0.64	76.4	2.94	0.86
This work	Pt-Co	66.6	0.80	0.27	0.53	0.18	74.2	0.46	0.23
This work	Pt/C	70.4	0.27	0.07	0.19	0.05	71.0	0.27	0.11
Ref.[40]	Pt-Pd-Cu	84	1.73	NA	0.50	NA	NA	2.20	0.45
Ref.[42]	Pt-Cu-Fe	75.5	1.37	NA	1.03	NA	NA	NA	NA
Ref.[63]	Pt-Pd-Au	NA	0.94	NA	1.14	NA	NA	NA	NA
Ref.[18]	Pt-Co-Au	NA	NA	0.75	NA	NA	NA	NA	NA
Ref.[21]	Pt-Ni-Mo	67.7	10.3	2.08	6.98	1.41	NA	8.20	1.74

View Article Online
DOI: 10.1039/C8TA00029H

Journal Name

ARTICLE

XPS survey spectra of the Pt-Co-W sample were conducted and the resultant outcomes are shown in Fig. S3. It shows the signatures of the Pt, Co, and W components respectively, illustrating the presence of the three metals. As shown in Table S2, the content of the W is 2.7 at%, which is almost in agreement with the result from ICP measurements (2.5 at%), revealing the doping of W into the Pt-Co system. In order to further study the element dispersion and alloying degree, the Pt-Co-W ternary alloy was characterized by scanning transmission electron microscopy (STEM) and X-ray spectroscopic (EDX) mapping. For the alloy, Its annular dark-filed scanning transmission electron microscopy (ADF-STEM) image of the Pt-Co-W alloy is shown in Fig. 1G, while the corresponding distribution mappings of Pt, Co and W elements are shown in Fig. 1H-J, respectively. As observed, the Pt, Co and W atoms are uniformly dispersed within the nanoparticle, indicating that the Pt-Co-W ternary alloy has a high alloying degree at an atomic level, which may contribute to the ORR activity.[42]

3.2. Catalytic activity of Pt-Co-W ternary alloy for ORR

To assess the electrochemical properties of the synthesized Pt-Co-W ternary alloy catalyst (20 wt% metal, relative to carbon), we performed cyclic voltammetry (CV) measurements to determine its electrochemically active surface area (ECSA) in an N_2-purged $HClO_4$ (0.1M) solution at a sweep rate of 50 $mV{\cdot}s^{-1}$. For comparison, the ECSAs of the Pt-Co bimetallic catalyst (20 wt% metal, relative to carbon) and a commercial Pt/C catalyst (the state-of-the-art 20 wt% Pt) as baseline catalysts have been determined under the same conditions. The obtained cyclic voltammograms for these above catalysts are shown in Fig. 2A. The ECSAs of these catalysts were calculated by the charge collected in the hydrogen adsorption/desorption region (between 0 V and 0.3 V) after double-layer correction and assuming a value of 210 $\mu C{\cdot}cm^{-2}$ for the adsorption of a hydrogen monolayer.[21] As depicted in Fig. 2B, the obtained ECSA of the Pt-Co-W catalyst is 65.9 $m^2g^{-1}Pt^{-1}$, which is comparable with that of the Pt-Co catalyst (66.6 $m^2g^{-1}Pt^{-1}$) and slightly lower than that of the commercial Pt/C (70.4 $m^2g^{-1}Pt^{-1}$). In order to further evaluate the electro-catalytic activity of the ternary alloy catalyst for ORR, the polarization curve was tested using a rotating-disk electrode (RDE) in an O_2-saturated 0.1M $HClO_4$ solution at a fixed rotation speed of 1600 rpm, as shown in Fig. 2C. At this rotation rate, for the Pt-based catalyst, the observed diffusion limiting current density is approximately 6.0 mA cm^{-2}, which is almost close to the theoretical one depicted in Fig. 2C. Surprisingly, the recorded half-wave potential of the Pt-Co-W catalyst is 0.97 V, which is much higher than that of the Pt-Co catalyst (0.91 V) or the commercial Pt/C (0.85 V), as shown in Fig. 2D. It illustrates the electro-catalytic activity of the synthesized Pt-Co-W ternary catalyst is the best among these catalysts. Moreover, the mass activity of Pt in the ternary alloy was calculated on the basis of the mass loading of Pt (14.18 $\mu g_{Pt}/cm^2$), at a fixed polarization potential 0.9 V, vs. reversible hydrogen electrode (RHE). The obtained mass activity of the Pt-Co-W catalyst is 2.25 $A{\cdot}mg^{-1}_{Pt}$, much higher than the mass activity of the Pt-Co bimetallic catalyst (0.53 $A{\cdot}mg^{-1}_{Pt}$), about 425 % higher than that of the Pt-Co alloy while approximately 12-fold enhancement than that obtained by the commercial Pt/C (0.19 $A{\cdot}mg^{-1}_{Pt}$), as depicted in Fig. 2E. More importantly, the synthesized Pt-Co-W catalyst possesses the highest specific activity (3.41 $mA{\cdot}cm^{-2}$) among all of the tested catalysts, which is nearly 4.3 or 13 times higher than that obtained by the Pt-Co bimetallic catalyst (0.80 $mA{\cdot}cm^{-2}$) or the commercial Pt/C (0.27 $mA{\cdot}cm^{-2}$), as shown in Fig. 2F. We also evaluated the catalytic performance using the ECSA values determined by CO stripping method (Fig. S4). In this case, the obtained specific activity of each of the tested Pt-based alloys is shown in Table1. As observed, the specific activities of Pt/C, Pt-Co and Pt-Co-W are 0.27$mA{\cdot}cm^{-2}$, 0.46 $mA{\cdot}cm^{-2}$ and 2.94 $mA{\cdot}cm^{-2}$, respectively. Among these catalysts, the Pt-Co-W also shows the best ORR activity, which is in accordance with the result based on the H_{upd}. All of the above results suggest that the Pt-Co-W ternary exhibits remarkably superior ORR activity to the Pt-Co binary alloy[13,43,44] as well as other reported Pt-based binary alloys such as PtNi, PtCu, etc shown in Table S3. As illustrated in Table 1, at 0.9 V vs. RHE, the ORR activity of the as-synthesized Pt-Co-W alloy is much higher than most of the recently reported Pt-based trimetallic catalysts but lower than the Pt-Ni-Mo catalyst (Mo-Pt_3Ni/C) that showing the best specific activity and the mass activity reported recently.[21] At 0.95 V vs. RHE, the recorded activity of the Pt-Co-W catalyst is lower than that of the Mo-Pt_3Ni/C, but it is still better than other catalysts, revealing an excellent performance at lower overpotentials. Among all the currently reported Pt-based catalysts, the Mo-Pt_3Ni/C exhibits the best ORR kinetic current by now, which is associated with an ultra-low loading of the catalyst (4.08 $\mu g_{Pt}/cm^2$) on working electrode that is much lower that of the Pt-Co-W catalyst (14.18 $\mu g_{Pt}/cm^2$) in this work and other Pt-based catalysts.[18,40,42,63] Unfortunatly, as we used the similar ultra-low loading like the Mo-Pt_3Ni/C catalyst, the full coverage on working electrode by the as-synthesized Pt-Co-W/graphene cannot been achieved in our case.

View Article Online
DOI: 10.1039/C8TA00029H

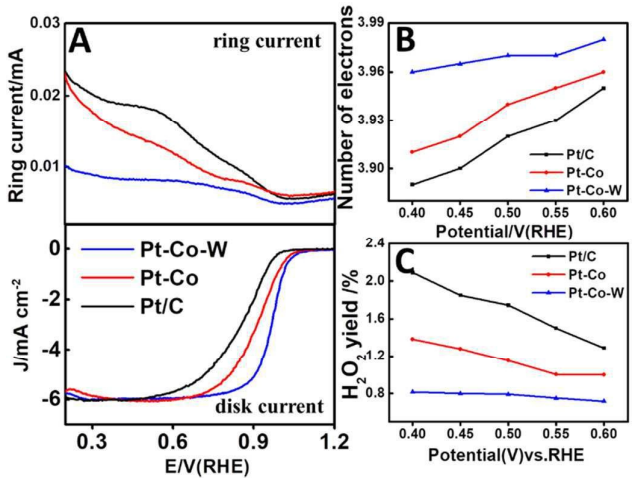

Fig. 3 (A) Rotating ring-disk electrode voltammograms recorded on all the catalysts in an O_2-purged 0.1M $HClO_4$ solution with the scan rate of 5 mV·s^{-1} at 1600 rpm; **(B)** The number of transferred electrons during ORR on the above catalysts, obtained at different polarization potentials; **(C)** The hydrogen peroxide yields on the catalysts.

In order to investigate the hydrogen peroxide yield for the ORR over the Pt-Co-W catalyst, we performed rotating ring-disk electrode (RRDE) measurements in the 0.1M $HClO_4$ solution saturated with O_2 at room temperature and the resulting outcomes are shown in Fig. 3. The ring and the disk currents are in the negative scan direction and the ring potential was fixed at 0.5 V vs. saturated calomel electrode (SCE). The Pt-Co catalyst and the commercial Pt/C were performed as references. As observed in Fig. 3A, the ring currents (Ir) of all the catalysts are very low compared to the corresponding disk currents (Id), indicating that low hydrogen peroxide yields on these catalysts. Furthermore, among these tested catalysts, the Pt-Co-W catalyst possesses the highest disk current (O_2 reduction) and the lowest ring current (HO_2^-), illustrating that the Pt-Co-W ternary alloy catalyst owns the lowest hydrogen peroxide yield and highest catalytic efficiency. In order to confirm the definite pathway of the ORR process, using the data of Fig. 3A, we calculated the number of transferred electrons (n) and the hydrogen peroxide yield, by using the following equations:

$$\mathrm{n} = 4\frac{Id}{Id + {Ir}/{N}}$$

$$HO_2^- = 200\frac{\frac{Ir}{N}}{\frac{Ir}{N} + Id}$$

Where Id, Ir, N are the disk current, the ring current, the current collection efficiency of RRDE (0.37), respectively. As shown in Fig. 3B and 3C, the negligible hydrogen peroxide production reveals that the Pt-Co-W ternary catalyst has a good ability to catalyze the ORR undergoing a fully 4-electron pathway, even at the high over-potential. The reason for the small atomic content of W that governs the electrochemical performance of the Pt-Co-W alloy may be attributed to a strong interaction between the oxophilic W and Pt, Co. The W may bond strongly with Pt and Co atoms to form strong W-Pt and W-Co bonds, which contribute to the performance of the Pt-Co-W system. For examining the effect of the W on the electrochemical performance of the ternary alloy, we synthesized the Pt-W binary catalyst for comparison. As shown in Fig. S5, the Pt-W catalyst shows a poor ORR activity with respect to the Pt-Co-W, revealing that the Co is indispensable for the ternary catalyst. But, the detail reasons need to be further investigated by changing the W contents in this alloy.

In addition, the Pt-Co-W trimetallic catalyst also exhibits a better durability in comparison than the Pt-Co bimetallic catalyst and the commercial Pt/C as baseline catalysts. The durabilities for the Pt-based catalysts are evaluated by the polarization curves in the N_2-purged 0.1M $HClO_4$ solution with the potential cycling between 0.2 V and 1.2 V versus RHE at 100 mV·s^{-1} for 1000 cycles. As illustrated in Fig. 4A-C, after 1000 cycles, the specific activity of the Pt-Co-W catalyst is almost changeless compared with the initial one. as shown in Fig. 4D. For comparison, the recorded specific activity of the Pt-Co and the commercial Pt/C catalysts obviously decrease after the durability tests. This reveals that the durability for the Pt-Co-W catalyst is superior to the Pt-Co or the Pt/C catalysts. To probe what happens to the Pt-Co-W alloy after some time-test in $HClO_4$, we checked the surface composition of the sample again. As shown in Fig. S6, the post XPS results show the content of the W or Co component is almost similar to that of the original sample, as evidenced by Table S4. For comparison, the contents of Pt and Co are declined for Pt-Co catalyst with respect to the Pt-Co-W catalyst (Fig. S7). To further study the stability of the Pt-Co-W catalyst, post operation TEM analysis after accelerated durability test (ADT) can be useful to evaluate the possible degradation phenomena. As shown in Fig. S8, the morphology of the Pt-Co-W catalyst is almost similar to that of the original one after ADT. No dissolution or particle growth phenomena have been found. Moreover, the change in the content of W or Co is negligible for the Pt-Co-W catalyst after ADT, confirmed by the ICP results (Table S6). Therefore, the outstanding stability of the Pt-Co-W catalyst can also be ascribed to the doping of the refractory 5d transition metal W into this alloys system. Since the oxophilic 5d transition metal W has very strong chemical affinity, there exists a strong interaction between the metal W and Pt, Co.[45-47] Due to the interactions between them, W can bond strongly with Pt and Co atoms to form strong W-Pt and W-Co bonds, which contribute to stabilize the Pt and Co in the Pt-Co-W system.[48,49] Therefore, taken together surprisingly high electro-catalytic activity, negligible hydrogen peroxide production, and outstanding durability for the ORR, the as-synthesized Pt-Co-W ternary alloy has been considered as one of the most competitive and efficient next-generation catalysts, alternative the expensive Pt catalyst in acidic environments.

View Article Online
DOI: 10.1039/C8TA00029H

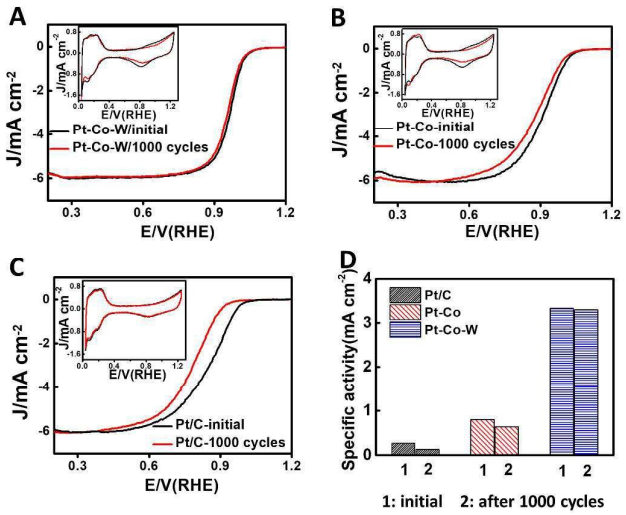

Fig. 4 Stability characterization of different catalysts including the Pt-Co-W, Pt-Co, and Pt/C catalysts before and after the accelerated durability test. **(A)** Pt-Co-W catalyst; **(B)** Pt-Co catalysts; **(C)** Commercial Pt/C; **(D)** The changes of specific activities of the catalysts before and after 1000 cycles.

3.3. The effect of W on the ORR kinetics

As one of the refractory non-precious transition metals, the

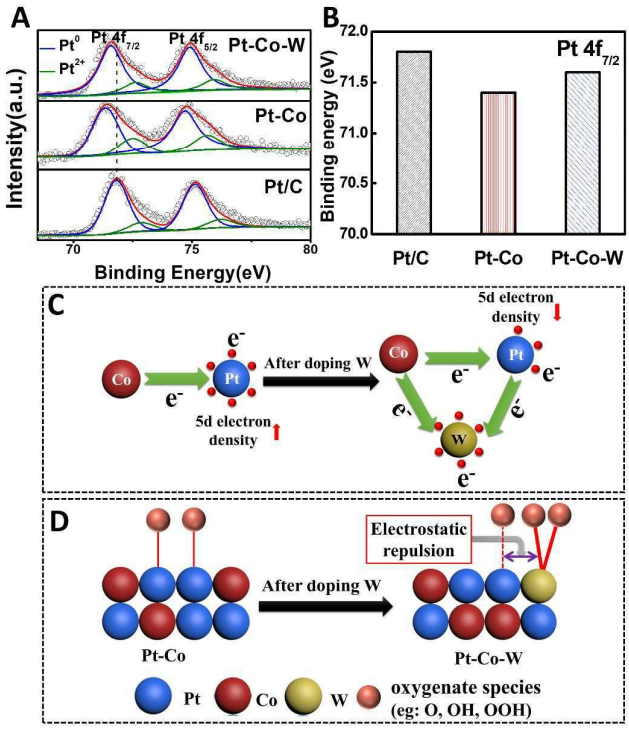

Fig. 5 (A) High resolution XPS spectra showing Pt 4f peaks deriving from the presence of different valence states. These include metallic Pt as majority and Pt(2+), such as PtO and $Pt(OH)_2$, in a lower content; **(B)** The Pt $4f_{7/2}$ core-level biding energies; **(C)** Schematic illustrates that the electronic structure of Pt is affected by the doped Co and W; **(D)** Schematic illustrates the enhanced desorption of oxidic species on the Pt-Co-W catalyst.

W has a strong electronegativity, lots of unsaturated 5d orbitals, and the high-valency states coordinated with oxygen.[28,50,51] As the W is added into the Pt-Co binary alloy system, the electronic structure of Pt atoms in the ternary system will substantially change, compared with Pt-Co alloy. To confirm this hypothesis, we conducted X-ray photoelectron spectroscopy (XPS) for the Pt-Co-W and Pt-Co catalysts, respectively. The resulting Pt 4f core-level binding energies are shown in Fig. 5A. The area ratio between fitted Pt $4f_{7/2}$ and Pt $4f_{5/2}$ peaks is fixed at 4:3 and the two peaks have equal full width at half maxima (FWHM) (Table S5), based on the degeneracy of each spin state according to the number of different spin combinations.[52-57] Moreover, the $4f_{7/2}$ is more intense than the $4f_{5/2}$ in the deconvoluted peaks due to spin-orbit splitting. For the synthesized alloy catalysts, the obtained B.E. values of the Pt $4f_{7/2}$ and Pt $4f_{5/2}$ peaks identified by Fig.5A are shown in Table 2. As observed, the recorded B.E. of Pt $4f_{7/2}$ or Pt $4f_{5/2}$ peak shifts to lower binding energy for the Pt-Co and Pt-Co-W alloys with respect to the Pt/C. For these Pt-based alloys, the negative shift of the B.E can be attributed to the addition of Co with much lower electronegativity than Pt, as reported by related literature[22,52-56]. Moreover, the percentage of the metallic Pt^0 is much more than that of the oxidative Pt (Pt^2) for all the Pt-based catalysts, this outcome is consistent with the published results available in the literature in Table 2.

However, the negative shift of Pt $4f_{7/2}$ in the Pt-Co-W ternary alloy is smaller than that of the binary alloy, as depicted by Fig. 5B and Table 2. This smaller downshift can be explained by the fact that the unfilled 5d ($5d^4$) of W can attract some electrons from the alloyed Pt, because the electronegativity of W (2.36) is much higher than that of Pt (2.28) or Co (1.88). Such electron transfer between the two metals will lead to the decrease in the 5d electron density of Pt atoms shown in Fig. 5C, resulting in the smaller downshift of the binding energy of Pt $4f_{7/2}$, even though the content of the W is minor in comparison with the majority of Co or Pt atoms in the Pt-Co-W alloy, as shown in Table S1. Besides the electron structure, the surface properties of the alloy catalysts are given in Fig. S9. For the Pt-Co-W catalyst, the surface Pt is mainly in the metallic state and the surface Co is in oxidized state of Co^{2+} or Co^{3+}, the majority of W is the oxidized states of W^{4+} and W^{6+}. For the Pt-Co sample, the surface Pt was mainly in the metallic state and the surface Co was in oxidized state of Co^{2+} and Co^{3+}. These results are in agreement with related references.[55-59]

It is generally believed that the negative shift in the binding energy of the Pt 4f core level reflects the downshift of its d-band centre, relative to the Fermi level.[60-62] For Pt-based alloys, the downshift of d-band centre generally exhibits two opposite effects on the ORR kinetics.[22] On the one hand, the downshifted d-band centre of Pt can weaken the chemical adsorption strength of active oxygen molecular, which can block O-O bond breaking and subsequently deteriorate the ORR kinetics. On the other hand, the downshifted d-band centre can also weaken the chemical adsorption strength of the oxygenated intermediates like O and OH species and then facilitate the desorption of these the oxygen-containing species, which lead to more electrochemically active sites

View Article Online
DOI: 10.1039/C8TA00029H

available for the ORR yet. So, there should be a balance between the two opposite effects involved the adsorption of active oxygen and desorption of these above intermediates, which should be responsible for the enhanced ORR activity. This conclusion can be verified by the fact that the Pt-Co binary alloy exhibits the better ORR activity to the Pt/C, as shown in Fig. 2.

However, the as-synthesized Pt-Co-W ternary system displays much higher ORR activity than that of the Pt-Co binary alloy shown in Fig. 2. It implies that the ORR mechanism catalyzed by the ternary catalyst is remarkably different from that of the Pt-Co in this case. First, compared with the Pt-Co bimetallic catalyst, the Pt-Co-W trimetallic system displays the smaller downshift of the binding energy of Pt 4f shown in Fig. 5B, illustrating that the active O_2 chemical adsorption becomes stronger and the O-O bonds breaking becomes easily, which subsequently facilitate the ORR kinetics. Second, because of the metal W having lots of unsaturated 5d orbitals ($5d^4 6S^2$), it can be expected to result in the charge redistribution by hybridization from the Pt to W atoms, which results in increased 5d vacancies of Pt. The increase in 5d vacancies can facilitate the chemical adsorption of active O_2 through the donation of 2π electrons from O_2 to Pt, which leads to the O-O bond breaking easily and the fast ORR rate. Also, the strong charge redistribution by hybridization between W and Pt atoms is beneficial to enhance the durability of Pt in its ternary catalyst through preventing the chemical dissolution of platinum, as verified by Fig. 4. Third, according to the reported results,[63,64] the addition of W can raise the oxygen adsorption strength of Pt and thus accelerate the breaking of O-O bond, but it also binds the OH_{ad} intermediates more strongly, which may make these intermediates desorption difficultly form Pt. However, different from 3d transition metals, such as Co, Fe, Ni, Cu and etc, the metal W is more active for chemisorbed oxygen-containing species (e.g.: O, OH, OOH) and the adsorption strength of these species on the W atoms is higher than that of Pt or Co.[32,33,65] There is a strong lateral repulsion between these oxygenated species adsorbed on the Pt and adjacent W atoms in the synthesized Pt-Co-W alloy,[66,67] which can result in the easy divorce of these species adsorbed on the Pt surface. Besides the lateral repulsion caused by the oxophilic properties of W, the steric effect, raised by the oxygenated species adsorbed on the Pt atoms and adjacent W atoms respectively, can also contribute to the removal of the oxygenated species from the active Pt surface, as shown in Fig.

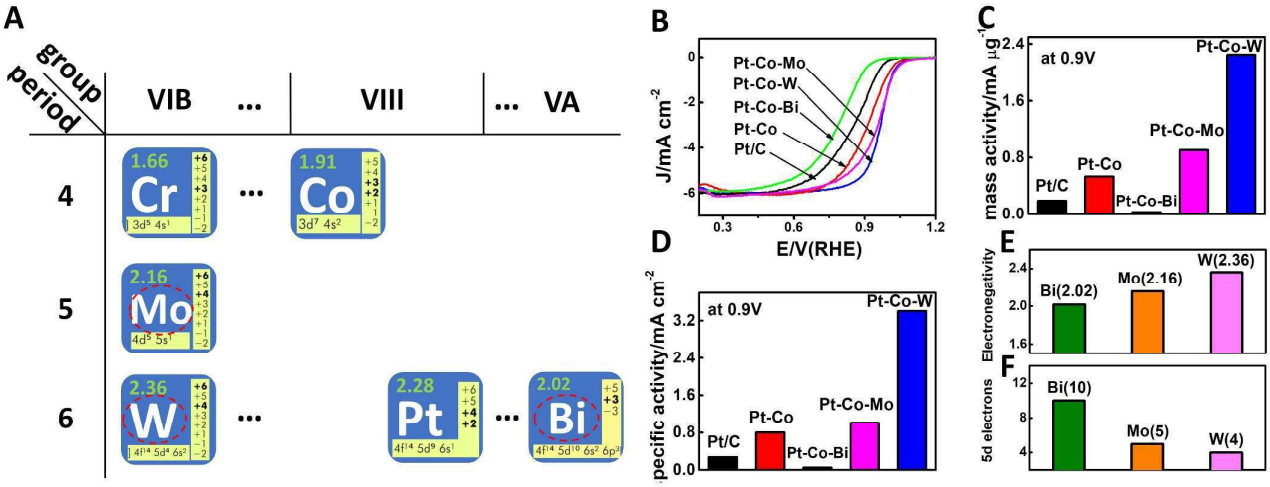

Fig. 6 (A) Fragmented periodic table showcasing promising candidates for the synthesis of Pt-based alloy catalysts. The green numbers: electronegativity; **(B)** RDE measurements of ORR on various catalyst samples in an O_2-purged 0.1M $HClO_4$ solution with a sweep rate of 5 $mV \cdot s^{-1}$ at 1600 rpm; **(C)** The mass activity of various catalyst samples; **(D)** The specific activity of various catalyst samples; **(E)** The electronegativity of transition metal Bi, Mo and W; **(F)** The 5d electrons of transition metal Bi, Mo and W.

Table 2 The binding energy values of Pt 4f peaks and the percentages of the main species identified by Fig.5A. (NA- not available)

		Binding energy (eV)		Pt^0 content (%)	Pt^{2+} content (%)
		Pt $4f_{7/2}$	Pt $4f_{5/2}$		
This work	Pt/C	71.8	75.1	81.8	18.2
	Pt-Co	71.4	74.8	72.1	27.9
	Pt-Co-W	71.6	74.9	79.9	20.1
Ref. 56	Pt/C	71.6	75.0	NA	NA
	Pt-Co	71.4	74.9	NA	NA
Ref. 22	Pt/C	71.9	75.2	80.5	19.5
	Pt-Co	71.8	75.1	73.7	26.3
Ref. 57	Pt/C	71.2	74.4	NA	NA
	TiNiN@Pt	70.8	74.2	NA	NA

View Article Online
DOI: 10.1039/C8TA00029H

5D. As a result, more electrochemically active sites available for the ORR over the Pt-Co-W alloy. In order to provide a direct proof for the strengthened desorption of oxygen-containing groups on the Pt-Co-W catalyst, a control experiment of the OH_{ads} trapping on it was conducted through the photoluminescence method by reacting terephthalic acid (TA) with OH immediately to produce highly fluorescent product.[68] As evidenced by Fig. S10, the ability of the OH_{ads} desorption from the Pt-Co-W catalyst is stronger than the Pt-Co alloy. This conclusion is inagreement with the results repored by Ding et al.,[69] who fabricated a Pt-Pd-Au trimetallic electrocatalyst and found that the significantly improved ORR activity (1.47A/mg_{Pt} at at 0.9V) and stability can be arributed to the easy removal of the adsorbed OH species on the catalyst surface, caused by alloying of the three metals.

3.4. Comparative analysis of W, Mo, Bi catalyzing the ORR kinetics

To further confirm the result that the addition of the refractory 5d transition metals like W can efficiently improve the ORR activity of Pt-Co binary alloy, we chosen refractory 4d transition Mo (same group with W) and non-refractory metal Bi (but same row with W) as third elements (Fig.6A) to synthesize graphene-supported Pt-Co-Mo and Pt-Co-Bi ternary alloys respectively, using the similar polyol reduction method for fabricating the Pt-Co-W. As shown in Fig. S11 and Fig. S12, the obtained ternary Pt-Co-Mo or Pt-Co-Bi alloy nanoparticles are highly dispersed on graphene support with a narrow particle size distribution. Also, the XRD results for the above two ternary alloys also show the formation of Pt-based solid solution alloys (Fig. S13). These results are similar to those of the Pt-Co-W ternary alloy (Fig. 1). Fig. 6B shows the ORR activities of these above ternary alloys. To further compare their ORR activities, the mass activity of each of the three alloys was determined by normalizing the mass of metal Pt, as shown in Fig. 6C. Afterward, based on the electrochemically active surface area (ECSA) measurements for these catalysts (Fig. S14), the specific activities of them are given in Fig. 6D. Taken together the mass and specific activities above, we can obvious observe that these ternary alloy catalysts show different ORR activity form each other. Estimated from the specific activity, their catalytic activities follow the order Pt-Co-W > Pt-Co-Mo > Pt-Co > Pt/C > Pt-Co-Bi, with the specific activity values of 3.41, 1.01, 0.80, 0.27, 0.05 $mA{\cdot}cm^{-2}$, respectively.

Based on this order of the activity for these catalysts, there exist some very interesting results. First, the ORR activity of the Pt-Co-Mo is slightly lower than that obtained by the Pt-Co-W but it is much higher than that obtained by the Pt-Co alloy. It reveals that, similar to the W, the addition of the metal Mo into the Pt-Co binary system can also facilitate the ORR kinetics, because Mo is one of the refractory non-precious transition metals like W that belongs to the similar Group □B. But, in comparison with the Pt-Co-W, its lower ORR activity can be associated with the fact that the electronegativity of Mo (2.16) is smaller than that of W (2.36) (Fig. 6D). Second, we also found the ternary Pt-Co-Bi alloy exhibits the lowest activity among all the Pt-based alloys, even lower than the commercial Pt/C. The poor activity is mainly attributed to the completely filled 5d orbitals ($5d^{10}$) of the non-refractory Bi, although its electronegativity is slightly lower than that of the W, as shown in Fig. 6D and 6E. All the above results reveal that the electronegativity and d-band electron density and valence state for non-precious transition metals play a synergistic role in enabling the catalytic activity of the Pt-based alloy catalysts. Based on this conclusion, it is expected that other refractory transition metals, such as Re, Ta and Hf with high electronegativity, unfilled 5d orbitals, and high valence state, may remarkably improve the ORR performance of Pt-based ternary alloys, if they are added into the binary alloy systems.

4. Conclusions

The graphene-supported Pt-Co-W ternary alloy is firstly prepared by varying the pH of the ethylene glycol solution containing H_2PtCl_6, $CoCl_2$ and $W(CO)_6$ as precursor salts, using one-pot polyol reduction method. The obtained well-defined Pt-Co-W alloy nanoparticles uniformly are distributed on the graphene surface with a narrow particle size distribution (2-3 nm). In 0.1M $HClO_4$ solutions, the as-synthesized ternary alloy exhibits the surprisingly improved mass activity (2.25 $A{\cdot}mg^{-1}_{Pt}$) and specific activity (3.41$mA{\cdot}cm^{-2}$), which are 425% and 118% higher than those obtained by the Pt-Co binary alloy (0.53 $A{\cdot}mg^{-1}_{Pt}$ and 0.80 $mA{\cdot}cm^{-2}$). Moreover, they are 11.8- and 12.6-fold higher than those obtained by a state-of-the-art commercial Pt/C catalyst (0.19 $A{\cdot}mg^{-1}_{Pt}$ and 0.27 $mA{\cdot}cm^{-2}$). The alloy catalyst also displays superior electrochemical durability during the ORR, compared with the other Pt-based catalyst. The remarkably enhanced ORR performances can be associated with the addition of low 5d transition metal tungsten into this Pt-Co alloy systems, which contributes the ORR kinetic process. The detail ORR mechanism over the Pt-Co-W ternary system is substantially different from that on the well-known Pt-Co binary alloy. On the one hand, sine W has a stronger electronegativity and higher unsaturated 5d orbitals than Pt or Co, the added W can result in the smaller downshift of the binding energy of Pt component in the Pt-Co-W ternary alloy with respect to the Pt-Co binary alloy, which would strengthens the chemical adsorption strength of active oxygen molecular. As a result, the O-O bond breaking easily and subsequently contributes the ORR kinetics. On the other hand, the transition metal W, as one of the high-valency metals, exhibits much stronger ligand with intermediates generated by the ORR, relative to Pt or Co atoms. The stronger ligand effect of the added W atoms can lead to easier divorce of these oxygenated intermediates adsorbed on the neighborhood Pt atoms through a lateral repulsion, resulting in more electrochemically active sites available for the ORR. The above results have been confirmed by the highly active Pt-Co-Mo and low active Pt-Co-Bi ternary alloys. Therefore, it is expected that introducing refractory transition metals, such as W, Ta and Hf with high-valency, unfilled d orbitals and strong electronegativity into Pt-based alloys, may open a door to

View Article Online
DOI: 10.1039/C8TA00029H

fabrication newly ultra-highly active next-generation catalysts for the ORR applied to fuel cell automotive.

Conflicts of interest

There are no conflicts to declare.

Acknowledgements

This work was supported by the National Natural Science Funds of China (No. 51572013, 51432003).

Notes and references

1 M. H. Shao, Q. W. Chang, *Chem. Rev.,* 2016, **116**, 3594-3657.
2 Y. H. Bing, H. S. Liu and L. Zhang, *Chem. Soc. Rev.*, 2010, **39**, 2184-2202.
3 B. J. Wang, *J. Power Sources,* 2005, **152**, 1-15.
4 E. J. Coleman, M. H. Chowdhury and A. C. Co, *ACS Catal.,* 2015, **5**, 1245-1253.
5 L. B. Venarusso, R. H. Sato, *J. Phys. Chem. C,* 2013, **117**, 7540−7551.
6 Y. J. Wang, N. N. Zhao, *Chem. Rev.,* 2015, **115**, 3433-3467.
7 B. P. Vinayan, R. I. Jafri, *Int. J. Hydrogen Energy,* 2012, **37**, 412-421.
8 K. S. Lee, T. Y. Jeon, *Appl. Catal. B: Environ.,* 2011,**102**, 334-342.
9 X. X. Du, Y. He, *Energy Environ. Sci.*, 2016, **9**, 2623-2632.
10 A. R. Seo, J. S. Lee, *Electrochimica Acta,* 2006, **52**, 1603-1611.
11 H. A. Gasteiger, S. S. Kocha, *Appl. Catal. B: Environ.,* 2005, **56**, 9-35.
12 B. Y. Xia, H. B. Wu, N. Li, *Angew. Chem. Int. Ed.,* 2015, **127**, 3868-3872.
13 D. C. Higgins, R. Y. Wang, M. A. Hoque, *Nano Energy*, 2014, **10**, 135-143.
14 S. J. Jiang, Y. W. Ma, *Adv. Mater.,* 2009, **21**, 4953-4956.
15 S. Chen, P. J. Ferreira, *J. Am. Chem. Soc.,* 2008, **130**, 13818-13819.
16 Q. H. Huang, H. Yang, *Electrochem. Commun.,* 2006, **8**, 1220-1224.
17 R. Srivastava, P. Mani, *Angew. Chem. Int. Ed.,* 2007, **46**, 8988-8991.
18 X. H. Tan, S. Prabhudev, A. Kohandehghan, ACS. Catal., 2015, **5**, 1513-1524.
19 J. L. Ferna´ndez, V. Raghuveer, A. Manthiram, A. J. Bard, *J. Am. Chem. Soc.,* 2005, **127**, 13100-13101.
20 Y. M. Zhou, D. M. Zhang, *J. Power Sources,* 2015, **278**, 396-403.
21 X. Q. Huang, Z. P. Zhao, *Sicence,* 2015, **348**, 1230-1234.
22 Y. G. Zhao, J. J. Liu, C. G. Liu, Y. Song and Wang, F. *J. Mater. Chem. A*, 2015, **3**, 20086-20091.
23 M. Chen, Z. B. Wang, *Electrochem. Commun.,* 2008, **10**, 443-446.
24 M. E. Scofield, C. Koenigsmann, *Energy Environ. Sci.*, 2015, **8**, 350-363.
25 S. Ozenler, N. Sahin, *ECS Trans.,* 2011, **41**, 1031-1042.
26 V. Stamenkovic, B. S. Mun, *Angew. Chem. Int. Ed.,* 2006, **118**, 2963-2967.
27 J. K. Nørskov, J. Rossmeisl, *J. Phys. Chem. B*, 2004, **108**, 17886-17892.
28 B. Zhang, X. L. Zheng, O. Voznyy, *Science,* 2016, **352**, 333-337.
29 S. J. Hwang, S. J. Yoo, *J. Phys. Chem. C,* 2011, **115**, 2483-2488.
30 Y. Wang, S.Q. Song, *Appl. Catal. B: Environ.,* 2009, **89**, 223-228.
31 M. GoÈ tz, H. Wendt, *Electrochimica Acta*, 1998, **43***,* 3637-3644.
32 K.C. Lee, L. Zhang, J.J. Zhang, *Electrochem. Commun.,* 2007, **9**, 1704-1708.
33 Y. Liu, C. Wen, Y. Guo, *J. Phys. Chem. C*, 2010, **114**, 9889-9897.
34 Y. G. Zhao,; J. J. Liu, Y. Song and Wang. F, *Phys. Chem. Chem. Phys.*, 2014, **16**, 19298- 19306.
35 L. F. Xiong, T. He, *Electrochem. Commun.,* 2006, **8**, 1671-1676.
36 M. B. Vukmirovic, J. Zhang, *Electrochimica Acta,* 2007, **52**, 2257-2263.
37 T. V. Cleve, S. Moniri, G. Belok, *ACS Catal.,* 2017, **7**, 17−24.
38 C. W. B. Bezerra, L. Zhang, *J. Power Sources,* 2007, **173**, 891-908.
39 A. U. Nilekar, Mavrikakis, M. *Surf. Sci.* 2008, **602**, L89-L94.
40 S. F. Fu, C. Z. Zhu, J. H.Song, *Nanoscale*, 2017, **9**, 1279-1284.
41 Y. Liang, H. Wang, P. Diao, W. Chang, G. Hong, Y. Li, M. Gong, L. Xie, J. Zhou, J. Wang, T. Z. Regier, F. Wei, H. Dai, *J. Am. Chem. Soc.*, 2012, **134**, 15849-15857.
42 H. Zhu, S. Zhang, S. J. Guo, *J. Am. Chem. Soc.*, 2013, **135**, 7130-7133.
43 Y. Nie, L. Li, Z. D. Wei, *Chem. Soc. Rev.,* 2015, **44**, 2168-2201.
44 P. Mani, R. Srivastava, P. Strasser, *J. Power Sources*, 2011, **196**, 666.
45 O. Alexeev, M. Shelef, B. C. Gates, *J. Catal.*, 1996, **164,** 1–15.
46 T. Maiyalagan, B. Viswanathan, *J. Power Sources*, 2008, **175**, 789–793.
47 B. Rajesh, V. Karthik, S. K. arthikeyan, K.R. Thampi, J.-M. Bonard, B. Viswanathan, *Fuel*, 2002, **81**, 2177-2190.
48 Y. I. Yermakov, B. N. Kuznetsov, V. A. Zakharov, "Catalysis by Supported Complexes." Elsevier, Amsterdam, 1981.
49 R. Arundhathi, T. Mizugaki, T. Mitsudome, K. Jitsukawa, K. Kaneda, *ChemSusChem*, 2013, **6**, 1345-1347.
50 R. B. Levy, M. Boudart, *Science,* 1973, **181**, 547-548.
51 M. V. Ganduglia-Pirovano, V. Natoli, M. H. Cohen, *Phys. Rev. B: Condens. Matter* 1996, **54**, 8892-8898.
52 V. T. Ho, C. J. Pan, J. Rick, W. N. Su, B. J. Hwang, *J. Am. Chem. Soc.* 2011, **133**, 11716.
53 C. Wang, H. Daimon, S. H. Sun, *Nano Lett.* 2009, **9**, 1493.
54 C. Dong, C. Lian, S. Hu, Z. Deng, J. Gong, M. Li, H. Liu,M. Xing, J. Zhang, *Nat. commun.,* 2018, **9**, 1-11.
55 L. Guo, W. Jiang, Y. Zhang, J. Hu, Z. Wei, L. Wan, *ACS Catal.* 2015, 5, 2903−2909.
56 A.S. AricoÁ, A.K. Shuklab, H. Kimc, S. Parkc, M. Minc, V. Antonucci, *Applied Surface Science,* 2001, **172**, 33-40.
57 X. Tian, J. Luo, H. Nan, H. Zou, R. Chen, T. Shu, X. Li, Y. Li, H. Song, S. Liao, R. R. Adzic, *J. Am. Chem. Soc.* 2016, 138, 1575−1583.
58 O.Yu. Khyzhun, *J. Alloy. Compd*., 2000, 305, 1-6.
59 F.Y. Xiea, L. Gonga, X. Liub, Y.T. Tao b, W.H. Zhanga, S.H. Chenb, H. Mengc, J. Chen, *J. Electron. Spectrosc. Relat. Phenom.,* 2012, 185, 112-118.
60 J. Wojciech, W. E. Morgan, *Inorg. Chem.,* 1972, **11**, 219-225.
61 F. H. B. Lima, J. Zhang and M. H. Shao, *J. Phys. Chem. C,* 2007**, 111**, 404-410.
62 B. Hammer, Y. Morikawa, *Phys. Rev. Lett.,* 1996, **76**, 2141-2144.
63 J. Greeley, I. E. L. Stephens, A. S. Bondarenko, T. P. Johansson, H. A. Hansen , T. F. Jaramillo, J. Rossmeisl , I. Chorkendorff, J. K. Nørskov, *Nat. Chem*., 2009, **1**, 552-556.
64 T. Fu, J. Fang, C. Wang, J. Zhao, *J. Mater. Chem. A*, 2016, **4**, 8803-8811.
65 U. A. Paulus, A. Wokaun and G. G. Scherer, *J. Phys. Chem. B,* 2002, **106***,* 4181-4191.
66 J. L. Zhang, M. B. Vukmirovic, *J. Am. Chem. Soc.,* 2005, **127**, 12480-12481.
67 A.U. Nilekar, Y. Xu, *Top Catal.,* 2007*,* **46***,* 276-284.

View Article Online
DOI: 10.1039/C8TA00029H

68 Y.L. Chen, Z. H. Ai, L. Z. Zhang, *J. Hazard. Mater.* 2012, **92**, 235-236.
69 J. Li, H. M. Yin, X. B. li, Y. Ding, *Nature Energy*, 2017, **2**, 17111.

View Article Online
DOI: 10.1039/C8TA00029H

Adding refractory 5d transition metal W into PtCo system: An advanced ternary alloy for efficient oxygen reduction reaction

Yijun Wu, Yige Zhao, Jingjun Liu*, Feng Wang*

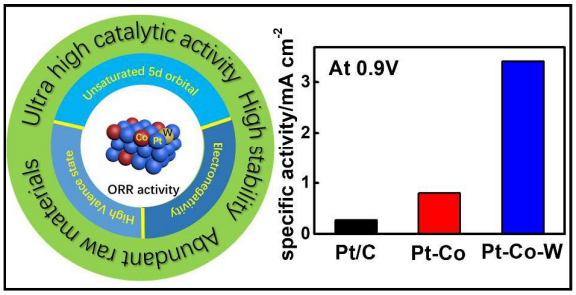

Schematic diagram of the Pt-Co-W catalyst with remarkably enhanced ORR activity than the Pt/C.